

# R13, a TrkB Agonist Prodrug, Inhibits Asparagine Endopeptidase (AEP) and Increases Osteoprotegerin (OPG), Preventing Bone Loss

**Jing Xiong**

Emory University

**Xia Liu**

Emory University

**Zhaohui Zhang**

Wuhan University

**Jonathan Adams**

Emory university

**Roberto Pacifici**

Emory University <https://orcid.org/0000-0001-6077-8250>

**Keqiang Ye** (✉ [kye@emory.edu](mailto:kye@emory.edu))

Emory University <https://orcid.org/0000-0002-7657-8154>

---

## Article

**Keywords:** BDNF, TrkB, R13, osteoporosis

**Posted Date:** April 23rd, 2021

**DOI:** <https://doi.org/10.21203/rs.3.rs-412961/v1>

**License:** © ⓘ This work is licensed under a Creative Commons Attribution 4.0 International License.

[Read Full License](#)

---

1 **R13, a TrkB Agonist Prodrug, Inhibits Asparagine Endopeptidase (AEP) and Increases**  
2 **Osteoprotegerin (OPG), Preventing Bone Loss**

3  
4 By

5  
6 Jing Xiong<sup>1,2</sup>, Xia Liu<sup>1</sup>, Zhaohui Zhang<sup>2</sup>, Jonathan W. Adam<sup>3</sup>, Roberto Pacifici<sup>3</sup> and  
7 Keqiang Ye<sup>1, #</sup>

8  
9 <sup>1</sup>Department of Pathology and Laboratory Medicine,

10 <sup>3</sup>Division of Endocrinology, Metabolism and Lipids, Department of Medicine,

11 Emory University School of Medicine

12 Atlanta, GA 30322,

13 USA

14 <sup>2</sup>Department of Neurology, Renmin Hospital of Wuhan University,

15 Wuhan 430060, Hubei Province, P. R. China

16  
17 <sup>#</sup>To whom all correspondence should be addressed (E-mail: [kyc@emory.edu](mailto:kyc@emory.edu))

18 Keywords: neurotrophins; C/EBP $\beta$ ; AEP; RANKL; OPG; Bone loss

20 **Abstract**

21 **Brain-derived neurotrophic factor (BDNF) and its tropomyosin-related kinase B**  
22 **receptor (TrkB) are expressed in human osteoblasts and mediate fracture healing.**  
23 **BDNF/TrkB signaling activates Akt that phosphorylates and inhibits asparagine**  
24 **endopeptidase (AEP), which regulates the differentiation fate of human bone marrow**  
25 **stromal cells (hBMSC) and is altered in postmenopausal osteoporosis. Here we show**  
26 **that R13, a small molecular TrkB receptor agonist prodrug, inhibits AEP and promotes**  
27 **bone formation. Though both Receptor activator of nuclear factor kappa-B ligand**  
28 **(RANKL) and Osteoprotegerin (OPG) induced by ovariectomy (OVX) remain**  
29 **comparable between WT and BDNF +/- mice, R13 treatment significantly elevates OPG**  
30 **in both mice without altering RANKL, blocking trabecular bone loss. Moreover, OVX**  
31 **increases RANKL and OPG in WT and AEP KO mice with RANKL/OPG ratio lower**  
32 **in the latter than the former, attenuating bone turnover. 7,8-DHF, released from the**  
33 **prodrug R13, activates TrkB and its downstream effector CREB, which is critical for**  
34 **OPG augmentation. Consequently, 7,8-DHF represses C/EBP $\beta$ /AEP pathway, inhibiting**  
35 **RANKL-induced RAW264.7 osteoclastogenesis. Therefore, our findings support that**  
36 **R13 exerts its therapeutic efficacy toward osteoporosis via inhibiting AEP and**  
37 **escalating OPG.**

38

39 **Introduction**

40 Brain-derived neurotrophic factor (BDNF) belongs to the family of neurotrophins that play  
41 essential roles in the central nervous system (CNS) and are mainly expressed in central and

42 peripheral neuronal tissues<sup>1,2</sup>. However, BDNF is also synthesized and released from non-  
43 neuronal cells such as fibroblasts, osteoblasts, endothelial cells, monocytes and mast cells<sup>3,4</sup>.  
44 Plasma BDNF levels are increased in patients with osteoarthritis compared to healthy  
45 individuals<sup>5</sup>. BDNF is involved in osteoblast cell differentiation and stimulates  
46 bone/cementum-related proteins including alkaline phosphatase (ALP), bone morphogenetic  
47 protein-2 (BMP-2) and osteopontin (OPN) expression in cementoblasts<sup>6</sup>. Both BDNF and its  
48 TrkB receptor are present at various stages of the bone formation process, and they are  
49 upregulated in human osteoblasts and implicated in fracture healing<sup>7</sup>. BDNF strongly  
50 elevates mRNA expression of the osteoblast differentiation marker, osteocalcin, in the  
51 osteoblast-lineage cell MC3T3-E1 and stimulates cell differentiation and promotes new bone  
52 formation and maturation<sup>8</sup>.

53  
54 AEP (asparaginyl endopeptidase, also known as legumain with gene name: *LGMN*) is a  
55 broadly expressed endo-lysosomal cysteine protease that is secreted as inactive pro-zymogen  
56 (56 kDa) and processed into an enzymatically active 36 kDa mature form and a 17 kDa C-  
57 terminal inhibitory fragment<sup>9</sup>. Strikingly, the C-terminal truncate inhibits osteoclast  
58 differentiation through binding to an uncharacterized receptor<sup>10,11</sup>. Active AEP inhibits  
59 osteoblast differentiation and *in vivo* bone formation through degradation of the bone matrix  
60 protein, fibronectin. During development, AEP-deficient zebrafish exhibits precocious bone  
61 formation and mineralization<sup>12</sup>. Human bone marrow stromal cells (hBMSCs) are non-  
62 hematopoietic multipotent cells capable of differentiation into mesodermal cell types such as  
63 osteoblasts and adipocytes<sup>13</sup>. Markedly, AEP regulates the lineage commitment of hBMSCs

64 and is abnormally expressed and displays aberrant subcellular localization in the bone from  
65 patients with postmenopausal osteoporosis<sup>12</sup>.

66

67 We have described 7,8-dihydroxyflavone (7,8-DHF) as a small molecule that mimics BDNF  
68 and acts as a specific TrkB agonist with high binding affinity. After binding to the  
69 extracellular motif on TrkB receptor, 7,8-DHF triggers receptor dimerization and auto-  
70 phosphorylation, initiating neurotrophic activities<sup>14-16</sup>. It is well documented that 7,8-DHF  
71 simulates BDNF biologic functions and exerts promising therapeutic efficacy toward a  
72 variety of diseases implicated with BDNF/TrkB signaling<sup>17-20</sup>. To improve its *in vivo*  
73 pharmacokinetic (PK) profiles, we have prepared a prodrug, R13, that releases 7,8-DHF after  
74 absorption and significantly increases its oral bioavailability<sup>21-23</sup>. Recently, we reported that  
75 BDNF/TrkB signaling inhibits AEP via Akt phosphorylation of the T322 residue,  
76 suppressing AEP activation<sup>24</sup>. Oral administration of R13 elicits robust TrkB receptor  
77 activation in the brain and the gut and inhibits AEP via Akt-mediated T322 phosphorylation  
78 <sup>21</sup>. Moreover, C/EBP $\beta$  is a pivotal transcription factor for escalating AEP expression during  
79 age<sup>25</sup>, and activation of the BDNF/TrkB pathway represses C/EBP $\beta$ /AEP signaling<sup>26</sup>.

80

81 Osteoporosis is a systemic bone disease, characterized by reduced bone mass, and disruption  
82 of normal bone architecture, resulting in bone fragility and increased risk of fractures<sup>27</sup>.

83 Bone homeostasis depends on the resorption of bones by osteoclasts and formation  
84 of bones by the osteoblasts. Osteoblasts can also affect osteoclast formation, differentiation,  
85 or apoptosis through several pathways, such as OPG/RANKL/RANK. In the current study, to

86 test the hypothesis that the BDNF mimetic drug R13 may block AEP and promote bone  
87 formation, we employed BDNF +/-, AEP -/- and wild-type (WT) littermate mice and  
88 examined their roles in ovariectomy (OVX)-induced bone loss in the presence or absence of  
89 R13. We found that AEP KO decreased OVX-induced bone loss via increasing osteoblast  
90 formation and inhibiting osteoclast formation. 7,8-DHF, the active pharmaceutical ingredient  
91 released from R13, elevates OPG expression via activating CREB and blocks RANKL-  
92 induced osteoclastogenesis. R13 not only represses AEP expression through blunting its  
93 upstream transcription factor C/EBP $\beta$  but also blocks AEP activation via BDNF/TrkB  
94 pathway-activated Akt and it displays promising therapeutic efficacy toward osteoporosis.

95

## 96 **Results**

### 97 **Knockout of AEP improves trabecular bone density in ovariectomized female mice**

98 To explore the role of AEP in bone remodeling, we subjected AEP knockout mice (AEP KO)  
99 and WT littermates to OVX at the age of 12 weeks. As expected, the shrunken uterine  
100 morphology and reduced uterus weight revealed that OVX surgery was successful  
101 (Supplementary Figure 1). Microcomputed tomography ( $\mu$ CT) analysis of femurs harvested  
102 at sacrifice revealed a higher trabecular bone volume fraction (BV/TV), Conn.D and a lower  
103 Structure model index (SMI) in AEP KO mice compared with AEP WT mice after OVX.  
104 Moreover, OVX decreased trabecular number (Tb.N) and increased trabecular separation  
105 (Tb.Sp), while trabecular thickness (Tb.Th) indices were similar among the groups. These  
106 indices remained similar between two types of mice under sham operation (Figure 1A & B).  
107 Notably, levels of serum osteocalcin, a marker of bone formation, were increased after OVX

108 with AEP KO significantly higher than WT. The serum [BDNF]s were comparable among  
109 the 4 groups. Quantification of bone resorption indices in the serum showed that the  
110 concentrations of C-terminal telopeptide of collagen (CTX), a marker for bone resorption,  
111 and RANKL were increased after OVX mice. Moreover, OPG concentrations were much  
112 higher in AEP KO mice than WT mice under both OVX and sham conditions, suggesting that  
113 AEP antagonizes OPG expression under the physiological condition. Consequently, the ratios  
114 of RANKL/OPG were substantially higher in OVX groups than sham groups with AEP KO  
115 mice lower than WT mice, in alignment with higher bone density in AEP KO group versus  
116 WT group after OVX (Figure 1C). Hence, AEP deletion diminishes the ratio of  
117 RANKL/OPG, leading to increased trabecular bone density after OVX.

118

### 119 **Deletion of AEP inhibits the bone turnover induced by ovariectomy**

120 To further characterize the roles of AEP in OVX-induced osteoporosis, we performed the  
121 H&E staining and analyzed the bone morphology and white adipocytes in both animals after  
122 OVX surgery. White adipocytes were evidently reduced in the bone from AEP KO mice after  
123 OVX as compared to WT mice (Figure 2A). Tartrate-resistant acid phosphatase (TRAP)  
124 staining revealed that OVX induced more osteoclast cells in WT than AEP KO mice (Figure  
125 2B). Based on dynamic indices of femur trabecular bone formation, no significant difference  
126 in mineral apposition rate (MAR) and bone formation rate (BFR) was found between WT and  
127 AEP KO sham mice, but OVX decreased the BFR in WT mice as compared with AEP KO  
128 mice (Fig. 2D). Analysis of static indices of bone formation and resorption revealed that both  
129 number of osteoclasts (N. Oc/BS) and the percentage of surfaces covered by osteoclasts

130 (OcS/BS) were greatly decreased in AEP KO mice compared with WT mice after OVX. On  
131 the other hand, OVX also elicited a compensatory increase of number of osteoblasts (N.  
132 Ob/BS) in AEP WT group but not in AEP KO mice (Figure 2D). Together, these data suggest  
133 that AEP deficient mice exhibit a higher bone formation and a lower bone resorption after  
134 OVX.

135

### 136 **R13 increases OPG levels and blocks trabecular bone loss induced by ovariectomy**

137 To explore the biological roles of BDNF/TrkB signaling in OVX-induced bone loss, we  
138 employed 3 months old female BDNF +/- mice and WT littermates. One week after OVX  
139 surgery, WT and BDNF +/- mice were administered either R13 (21.8 mg/kg) or vehicle,  
140 orally, six days per week for eight weeks. Assessment of femoral bone structure by *in vitro*  
141  $\mu$ CT revealed that trabecular bone volume, expressed as a function of total tissue volume  
142 fraction (BV/TV) was dramatically decreased by OVX in both WT and BDNF +/- mice. R13  
143 treatment increased BV/TV. Quantification of parameters of trabecular structure revealed that  
144 R13-treated mice displayed higher trabecular thickness (Tb.Th) than vehicle control and  
145 trabecular number (Tb.N), decreased trabecular spacing (Tb.Sp) in both type of mice as  
146 compared with the OVX-treated group (Figure 3A & B). Assessments of the serum levels of  
147 CTX and osteocalcin indicated osteocalcein was increased in R13-treated OVX mice  
148 compared with vehicle-treated OVX group, and both strains of OVX-treated mice exhibited  
149 higher CTX level compared to the sham group. Nevertheless, OPG were substantially  
150 increased upon R13 treatment, leading to significant reduction RANKL/OPG ratios in both  
151 WT and BDNF +/- mice, though the serum BDNF levels remained equivalent among the



152 groups (Figure 3C). Hence, BDNF haploinsufficiency does not alter femur trabecular bone  
153 properties after OVX, but treatments with R13 strongly increase bone density.

154

### 155 **R13 blocks the changes in bone turnover induced by ovariectomy**

156 To further explore the roles of BDNF signaling in bone resorption and formation after OVX,  
157 we conducted H&E staining and analyzed bone morphology and white adipocytes in both  
158 WT and BDNF<sup>+/-</sup> mice after OVX surgery. Clearly, R13 treatment decreased the adipocyte  
159 content in the bone after OVX (Figure 4A). TRAP staining revealed that OVX-induced  
160 demonstrable osteoclast cells in both WT and BDNF <sup>+/-</sup> mice were diminished by R13  
161 treatments (Figure 4B). Calcein double-fluorescence labeling allows the determination of the  
162 onset time and location of mineralization and the direction and speed of bone formation.  
163 Interestingly, R13 vigorously increased these parameters in both WT and BDNF <sup>+/-</sup> mice  
164 (Figure 4C), indicating that OVX-induced bone loss is attenuated by R13 treatment via an  
165 increase in bone formation. Dynamic indices of bone formation showed that vehicle-treated  
166 mice exhibited lower MAR and BFR as compared to R13-treated mice. By contrast, no  
167 significant differences in ObS/BS and N.Ob/BS, which are static indices of bone formation,  
168 were found in vehicle and R13-treated mice. Treatments with R13 inhibited N.Oc/BS in both  
169 WT and BDNF <sup>+/-</sup> mice after OVX. Nonetheless, the percentage of surfaces covered by OCs  
170 (Oc.S/BS) remained comparable among the groups regardless of the treatment (Figure 4D).  
171 Hence, these data support that R13 treatment induces bone formation and inhibits bone  
172 resorption after OVX. Remarkably, R13 significantly increased OPG levels without affecting  
173 RANKL and it also elevated BV/TV ratio in WT mice without any surgery (Supplementary

174 Figure 2). Thus, R13 treatment greatly blocks the bone loss induced by OVX and  
175 substantially elevates OPG levels.

176

### 177 **7,8-DHF promotes MC3T3-E4 cell differentiation, mineralization and OPG secretion**

178 7,8-DHF binds to TrkB receptor extracellular region, where BDNF interacts on the TrkB  
179 receptors<sup>28</sup>, mimicking the biological actions of BDNF in a TrkB-dependent manner<sup>29,30</sup>. To  
180 examine the molecular mechanisms of how 7,8-DHF stimulates bone density elevation in  
181 rodents, we tested its effect in MC3T3-E1 cells in the presence of OIM (osteogenic induction  
182 medium). Alkaline phosphatase (ALP) staining showed that OIM treatment at 14 days  
183 evidently enhanced osteoblast cell differentiation, which was further escalated by BDNF or  
184 7,8-DHF, respectively. Alizarin Red staining also validated these observations at 21 days  
185 (Figure 5A & B), supporting the conclusion that BDNF or 7,8-DHF strongly stimulates  
186 MC3T3-E1 differentiation and calcium deposition.

187

188 Stimulation of the BDNF/TrkB pathway inhibits AEP activation via Akt phosphorylation of  
189 T322 residue, sequestering AEP into the lysosomes<sup>24</sup> and decreases AEP expression levels  
190 via repressing its transcription factor C/EBP $\beta$ <sup>26</sup>. Immunoblotting revealed that OIM robustly  
191 induced p-C/EBP $\beta$  and total C/EBP $\beta$  expression in MC3T3-E1 cells, both of which were  
192 distinctly repressed by either BDNF or 7,8-DHF. Consequently, expression of the  
193 downstream effector, AEP, was clearly diminished, which inversely associated with RANKL  
194 and OPG augmentation. Osterix, a key early gene in the bone formation cascade, is usually  
195 used as a predictive measure of bone formation. As expected, OIM prominently elevated

196 Osterix levels as compared with vehicle. The similar findings occurred in the presence of  
197 BDNF or 7,8-DHF (Figure 5C & D). In alignment with active AEP repression by BDNF or  
198 7,8-DHF, the enzymatic assay validated that AEP protease activities were greatly blocked  
199 (Figure 5E).

200

201 To further interrogate the role of AEP in MC3T3-E1 cell differentiation and mineralization  
202 induced by OIM, we transfected the cells with dominant-negative enzymatic-dead AEP  
203 C189S mutant, and found that blockade of AEP highly escalated fibronectin, Osterix and  
204 RUNX2 (Supplementary Figure 3A & D). ALP staining and Alizarin Red S analysis showed  
205 that antagonizing AEP strongly promoted osteoblast cell differentiation and bone formation  
206 (Supplementary Figure 3B & C). As expected, AEP C189S mutant robustly inhibited OIM-  
207 elicited AEP activities (Supplementary Figure 3E). Quantitative RT-PCR (qRT-PCR)  
208 analysis revealed that 7,8-DHF exhibited the strongest stimulatory effect in promoting OPG  
209 mRNA levels, followed by BDNF and OIM. On the other hand, BDNF triggered the most  
210 RANKL mRNA transcription (Figure 5F). Both OPG and RANKL protein levels were  
211 elevated by OIM in ELISA assays. These elevations were further augmented in the presence  
212 of 7,8-DHF or BDNF (Figure 5G, left two panels), consistent with the findings in Western  
213 blotting. Though both RANKL and OPG concentrations were substantially elevated by  
214 BDNF and 7,8-DHF, the ratio of RANKL/OPG triggered by OIM alone was significantly  
215 higher than 7,8-DHF (Figure 5F, right panel). Together, these observations strongly support  
216 that 7,8-DHF mimics BDNF and that both strongly escalate OPG expression and decrease  
217 RANKL/OPG ratio, accelerating osteoblast formation. Moreover, it also represses the

218 C/EBP $\beta$ /AEP pathway, leading to inhibition of osteoclast formation.

219

### 220 **7,8-DHF increases OPG expression via activating transcription factor CREB**

221 To further interrogate the molecular mechanism of 7,8-DHF in promoting OPG expression,

222 we conducted a time course study in MC3T3-E1 cells in the presence of OIM. As expected,

223 7,8-DHF swiftly activated p-TrkB and its downstream effectors p-MAPK and p-Akt,

224 supporting that 7,8-DHF indeed mimics BDNF by activating TrkB neurotrophic signaling.

225 Numerous transcription factors including c-Jun and CREB have been shown to be implicated

226 in OPG mRNA transcription<sup>31,32</sup>. Noticeably, p-C/EBP $\beta$ , p-c-Jun and p-CREB signals were

227 time-dependently increased by 7,8-DHF (Figure 6A & B), suggestive of the activation of

228 these transcription factors. To examine which of them are essential for OPG expression, we

229 knocked down each of them in MC3T3-E1 cells via the specific siRNAs in the presence of

230 OIM and 7,8-DHF. Consistently, OIM manifestly increased OPG and RANKL, associated

231 with C/EBP and c-Jun augmentation, whereas CREB total level remained constant. Again,

232 7,8-DHF treatment attenuated C/EBP $\beta$  without interfering CREB or c-Jun levels.

233 Remarkably, knocking down CREB or c-Jun but not C/EBP $\beta$  clearly reduced OPG protein

234 levels, and the ratio of RANKL/OPG was significantly augmented when CREB was depleted

235 (Figure 6C & D). qRT-PCR demonstrated that 7,8-DHF-stimulated OPG mRNA was

236 selectively suppressed when CREB was knocked down by its siRNA, whereas RANKL

237 mRNA levels were similar among the groups, resulting in higher RANKL/OPG ratio (Figure

238 6E). Hence, 7,8-DHF via activating CREB, a well-characterized downstream transcription

239 factor of BDNF/TrkB pathway, stimulates OPG expression levels.

240

241 **7,8-DHF inhibits RANK-L-induced RAW264.7 osteoclastogenesis**

242 RAW264.7 cell is a well-established cellular model for osteoclastic differentiation, which has  
243 been widely engaged in bone homeostasis research. Moreover, RANKL independently  
244 induces RAW264.7 cell osteoclastic differentiation, which efficiently generates osteoclasts *in*  
245 *vitro*<sup>33</sup>. To investigate whether the promotion of bone formation by 7,8-DHF also might  
246 involve inhibiting osteoclastogenesis, we employed RAW264.7 cells in the presence of  
247 RANKL. Treatment with 30 ng/ml RANKL at day 4 significantly increased the number of  
248 multinucleated osteoclastic cells and this increase was diminished by addition of BDNF or  
249 7,8-DHF, indicating the inhibition of the ability of RANKL to promote osteoclastogenesis  
250 (Supplementary Figure 4A). Immunoblotting analysis revealed that C/EBP $\beta$  was greatly  
251 reduced by 7,8-DHF or BDNF treatments, and RANKL-stimulated AEP oscillated the  
252 upstream C/EBP $\beta$  levels (Supplementary Figure 4B & C). Hence, 7,8-DHF blocks RANKL-  
253 induced RAW264.7 osteoclastogenesis associated with AEP inhibition.

254

255

256 **Discussion**

257 BDNF stimulates mRNA expression of the osteoblast differentiation marker, osteocalcin, and  
258 promotes the differentiation of MC3T3-E1 cells, augmenting new bone formation and  
259 maturation<sup>8</sup>. Both BDNF and its TrkB receptor are demonstrable in various stages of the  
260 bone formation process in human fracture gap tissues and upregulated in human osteoblasts  
261<sup>7</sup>. However, we found that BDNF +/- mice fail to exhibit any significant difference in bone

262 loss from WT littermates upon OVX, indicating that endogenous BDNF/TrkB pathway might  
263 be dispensable in preventing bone loss triggered by OVX. Nevertheless, TrkB receptor  
264 agonist R13 treatment substantially elevates OPG and reduces RANKL/OPG ratios in both  
265 WT and BDNF +/- mice after OVX, leading to prominent bone density augmentation (Figure  
266 5&6). Previous study shows that central BDNF deletion produces a marked skeletal  
267 phenotype characterized by increased femur length, elevated whole bone mineral density, and  
268 bone mineral content. Moreover, the skeletal changes are developmentally regulated and  
269 appear concurrently with the metabolic phenotype, suggesting that the metabolic and skeletal  
270 actions of BDNF are linked<sup>34</sup>. Nonetheless, we did not find any significant bone alteration in  
271 BDNF +/- mice as compared to WT littermates (Figure 3). Presumably, complete BDNF  
272 knockout in the CNS may disrupt the endocrine hormones that mediate the metabolism and  
273 bone homeostasis.

274

275 The proinflammatory cytokines (e.g., TNF- $\alpha$  and IL-6) are upregulated in osteoporotic bone  
276 marrow microenvironment<sup>35</sup>. These cytokines activate the transcription factor C/EBP $\beta$ ,  
277 which feeds back and acts as transcription factor for these cytokines as well<sup>36</sup>. Most recently,  
278 we show that BDNF and C/EBP $\beta$  mutually regulate each other negatively. For instance,  
279 BDNF deficiency increases production of inflammatory cytokines and activates the  
280 JAK2/STAT3 pathway, resulting in the upregulation of transcription factor C/EBP $\beta$ <sup>26</sup>. In  
281 turn, C/EBP $\beta$  acts a repressor that binds to BDNF exon IV promoter and blocks BDNF  
282 mRNA transcription<sup>37</sup>. Treatments with BDNF and 7,8-DHF thus pronouncedly diminish  
283 C/EBP $\beta$  expression, leading to AEP reduction, which is inversely correlated with RANKL

284 and OPG escalation (Figure 5&6; supplementary Figure 4). Interestingly, we observed OPG  
285 elevation in AEP KO mice as compared to WT mice under sham condition (Fig 1C),  
286 suggesting that AEP somehow physiologically represses OPG expression. Previously, we  
287 reported that AEP cuts  $\alpha$ -Synuclein N103 and Tau N368, which bind to the TrkB receptor  
288 intracellular domain and inhibit the neurotrophic activities<sup>38,39</sup>. Conceivably, AEP  
289 antagonizes BDNF/TrkB neurotrophic signalings, leading to OPG suppression. Depletion of  
290 AEP consequently alleviates the inhibition and escalates OPG expression. OPG plays a  
291 suppressive role in cytokine-induced osteoclastogenesis<sup>40</sup>. Moreover, both CREB and c-fos  
292 transcription factors mediate OPG and RANKL mRNA expression<sup>31</sup>. Notably, CREB, a  
293 crucial downstream transcription factor of BDNF/TrkB pathway, plays a pivotal role in  
294 mediating 7,8-DHF-stimulated OPG escalation, though all of transcription factors including  
295 C/EBP $\beta$ , c-Jun and CREB are phosphorylated upon 7,8-DHF treatment, accompanied by p-  
296 TrkB and its downstream effectors escalation (Figure 6A & B). Thus, 7,8-DHF-triggered p-  
297 CREB is indispensable for augmenting OPG expression and osteoblast differentiation.

298

299 AEP is a secreted cysteine protease involved in diverse biological processes. The proteolytic  
300 activity of AEP is important for its effects on hBMSC differentiation and bone formation, and  
301 AEP inhibits osteoblast cell differentiation through degradation of fibronectin<sup>12</sup>. AEP  
302 expression is elevated in hBMSCs from osteoporotic patients and, at single-cell resolution,  
303 and AEP overexpression in adipocyte differentiation is inversely correlated with local  
304 trabecular bone volume. Recently, we have reported that C/EBP $\beta$  upregulates AEP expression  
305 during aging<sup>25</sup>. BDNF or 7,8-DHF robustly represses C/EBP $\beta$  expression induced by OIM

306 (Osteogenic induction medium) or RANKL, resulting in AEP reduction and its protease  
307 activity repression. Consequently, 7,8-DHF strongly blocked RANK-L induced RAW264.7  
308 osteoclastogenesis (Supplementary Figure 4). Remarkably, we have recently reported that  
309 7,8-DHF decreases follicle stimulatory hormone (FSH) production, resulting in increased  
310 serum estradiol in female mice treated with HFD <sup>41</sup>. Previously, it has been reported that FSH  
311 triggers bone loss and anti-FSH increased bone density without altering estrogen  
312 concentrations<sup>42,43</sup>. It is possible that FSH might somehow activate AEP and trigger bone  
313 loss. Imaginably, 7,8-DHF represses FSH production, resulting in AEP inhibition and bone  
314 density increase. Clearly, the data presented above, combined with AEP KO mice display  
315 diminished bone loss upon OVX and reduced RANKL/OPG ratios, strongly support the  
316 conclusion that R13 may ameliorate OVX-induced bone loss via antagonizing AEP and  
317 elevating OPG (Figure 6F).

318

## 319 **Methods**

### 320 **Animals**

321 Female C57BL6/J wild-type mice and BDNF<sup>+/-</sup> mice were obtained from Jackson  
322 Laboratory (MMRRC stock#000664 and 002267), then held and underwent breeding at  
323 Emory School of Medicine. The AEP knockout mice on a mixed C57BL/6 and 129/Ola  
324 background were generated as reported <sup>44</sup>. All *in vivo* experiments were carried out in female  
325 mice. All mice were kept under specific pathogen free conditions in an environmentally  
326 controlled clean room and housed at 22 °C on a 12-h/12-h light/dark cycle. Food and water  
327 were provided *ad lib*. The experiments were conducted according to the NIH animal care



328 guidelines and Emory School of Medicine guidelines. The protocol was reviewed and  
329 approved by the Institutional Animal Care and Use Committee (IACUC) at Emory  
330 University. WT, BDNF<sup>+/-</sup> mice, AEP WT and AEP knockout mice were bilaterally  
331 ovariectomized or sham operated at 12 weeks of age. One weeks after ovariectomy, the WT  
332 and BDNF<sup>+/-</sup> mice received vehicle or R13 dissolved in 5% DMSO/0.5% methylcellulose at  
333 dose of 21.8mg/kg/d, six days per week, for 8 weeks by gavage.

334

335 **Cell culture.** Murine MC3T3-E1 (subclone 4) cells and RAW 264.7 cells were obtained from  
336 American Type Culture Collection (ATCC, Manassas, VA, USA). The MC3T3-E1 cells were  
337 cultured in alpha-MEM (Gibco, cat. A1049001) with 10% FBS and 0.1% penicillin  
338 /streptomycin, but without ascorbic acid. The RAW 264.7 cells were cultured in DMEM  
339 supplemented with 10% FBS and 0.1% penicillin-streptomycin. The cells were maintained at  
340 37°C in a humidified atmosphere of 95% air and 5% CO<sub>2</sub>.

341

342 **Osteogenic differentiation.** MC3T3-E1 cells were seeded into plates in complete medium  
343 and cultured for 24 days until the cells reached 70% confluence. To initiate the  
344 differentiation, the cells were incubated in osteogenic induction medium (OIM) containing  $\alpha$ -  
345 MEM, 10% FBS, dexamethasone (10<sup>-7</sup>M),  $\beta$ -glycerophosphate (10 mM) and ascorbic acid  
346 (50  $\mu$ g/ml). The differentiation medium was replaced every 3 days, with DMSO, BDNF (50  
347 ng/ml) or 7,8 DHF (0.5  $\mu$ M) added into the medium. The MC3T3-E1 cells were transfected  
348 with AEPC189S plasmid, C/EBP  $\beta$  siRNA (sc-29862, Santa Cruz Biotechnology, USA),  
349 CREB siRNA (sc-35111, Santa Cruz Biotechnology, USA), C-Jun siRNA (sc-29224, Santa

350 Cruz Biotechnology, USA) or control plasmid or control-siRNA (sc-44237, Santa Cruz  
351 Biotechnology, USA) by Lipo3000 transfection reagent (Invitrogen, USA) according to the  
352 instructions.

353

354 **Osteoclast differentiation.** RAW264.7 cells were seeded in 24 wells plates and cultured for  
355 24 hours in DMEM with 10% FBS and 0.1 penicillin/streptomycin. The medium was  
356 changed to  $\alpha$ -MEM with 5% FBS, 0.1% penicillin/streptomycin. The receptor activator of  
357 NF- $\kappa$ B ligand (RANKL, 30 ng/ml) was added to induce osteoclast differentiation. The  
358 medium was replaced every 3 days, accompanied with DMSO, BDNF (50 ng/ml) or 7,8 DHF  
359 (0.5  $\mu$ M) added into the medium.

360

361 **ALP staining.** MC3T3-E1 cells were plated in 24-well plates, cultured in complete medium  
362 or OIM, and treated with BDNF (50 ng/ml) or 7,8 DHF (0.5  $\mu$ M) for 14 days. The Cells were  
363 washed in PBS twice, and fixed for 10 minutes with fixing buffer at room temperature,  
364 stained the ALP staining with the TRACP&ALP double-staining kit (TaKaRa, Japan, Cat.  
365 #MK300)

366

367 **Alizarin Red S staining.** MC3T3-E1 cells were treated with OIM, OIM + BDNF (50 ng/ml)  
368 or OIM + 7,8 DHF (0.5  $\mu$ M), and left untreated for 21 days, and then were washed in distilled  
369 water twice and fixed in 70% ice-cold ethanol. Then the cells were stained with 2% Alizarin  
370 Red S solution (Sigma, St. Louiss, MO, USA) to detect calcification.

371

372 **TRAP staining.** RAW 264.7 cells were cultured in  $\alpha$ -MEM with or without RANKL, in the  
373 presence or absence of BDNF (50 ng/ml) or 7,8 DHF (0.5  $\mu$ M) for 5 days. The cells were  
374 washed in PBS twice, fixed in fixing solution for 10 minutes at room temperature, and then  
375 stained the TRAP activity with the TRACP&ALP double-staining kit (TaKaRa, Japan, Cat.  
376 #MK300) according to the supplied protocols.

377

378 **Western blotting.** MC3T3-E1 and RAW 264.7 cells were washed with ice-cold PBS and  
379 lysed in (50 mM Tris, pH 7.4, 40 mM NaCl, 1 mM EDTA, 0.5% Triton X-100, 1.5 mM  
380  $\text{Na}_3\text{VO}_4$ , 50 mM NaF, 10 mM sodium pyrophosphate, 10 mM sodium  $\beta$ -glycerophosphate,  
381 supplemented with protease inhibitors cocktail) at 4°C for 0.5 h, and centrifuged for 25 min  
382 at 15,000 rpm. The supernatant was boiled in SDS loading buffer. After SDS-PAGE, the  
383 samples were transferred to a nitrocellulose membrane. The membrane was blocked with  
384 TBS containing 5% nonfat milk and 0.1% Tween 20 (TBST) at room temperature for 2 hours,  
385 followed by the incubation with primary antibody at 4°C overnight, and with the secondary  
386 antibody at room temperature for 2 hours. After washing with TBST, the membrane was  
387 developed using the enhanced chemiluminescent (ECL) detection system.

388

389 **AEP activity assay.** Cell lysates (10  $\mu$ g) were incubated in 200  $\mu$ l assay buffer (20 mM citric  
390 acid, 60 mM  $\text{Na}_2\text{HPO}_4$ , 1 mM EDTA, 0.1% CHAPS, and 1 mM DTT, pH 6.0) containing 20  
391  $\mu$ M  $\delta$ -secretase substrate Z-Ala-Ala-Asn-AMC (Bachem). AMC released by substrate  
392 cleavage was quantified by measuring at 460 nm in a fluorescence plate reader at 37 °C for 2  
393 h in kinetic mode.

394

395 **Quantitative real-time PCR analysis.** Total RNA was isolated by TRIzol (Life  
396 Technologies). Reverse transcription was performed with SuperScript III reverse transcriptase  
397 (Life Technologies). Gene-specific primers and probes were designed and bought from  
398 Taqman (Life Technologies). All real-time PCR reactions were performed using the ABI  
399 7500-Fast Real-Time PCR System and the Taqman Universal Master Mix Kit (Life  
400 Technologies). The relative quantification of gene expression was calculated using the  $\Delta\Delta C_t$   
401 method. We use predesigned real-time PCR primers from Applied Biosystems for the analysis  
402 of *Opg* (*Tnfrsf11b*; Mm0043545\_m1), *Rankl* (*Tnfsf11*; Mm00441908\_m1), *AEP* (*Lgmn*;  
403 Mm01325350\_m1), *GAPDH* (*Gapdh*; Mm99999915\_g1).

404

405  **$\mu$ CT measurements.**  $\mu$ CT scan and analysis was performed in femurs *ex vivo* using a  $\mu$ CT-40  
406 scanner, as previously reported<sup>45,46</sup>. Voxel sizes were 12  $\mu\text{m}^3$  for the *in vitro* measurements of  
407 femurs. For the femoral trabecular region, we analyzed 140 slices, beginning 50 slices below  
408 the distal growth plate. X-ray tube potential was 70 kVp, and integration time was 200 ms.  
409 Representative samples were reconstructed in 3D to generate visual representations of  
410 trabecular structure.

411

412 **Quantitative bone histomorphometry.** The measurements, indices and units for  
413 histomorphometric analysis were recommended by the Nomenclature Committee of the  
414 American Society of Bone and Mineral Research<sup>47</sup>. Mice were injected with calcein (25  
415  $\mu\text{g/g}$ ) subcutaneously at day 10 and day 3 before sacrifice. Bone histomorphometric analysis

416 was performed at the University of Alabama at Birmingham Center for Metabolic Bone  
417 Disease-Histomorphometry and Molecular Analysis Core Laboratory. The Goldner's  
418 trichrome-stained plastic-embedded sections of calcein-double labeled femora of the mice  
419 were analyzed by an operator blinded as to the nature of the samples.

420

421 **Biochemical markers of bone turnover.** Serum Osteocalcin (Novus biologicals, Cat. NBP2-  
422 68151), CTX (Immunodiagnostic systems, Cat. AC-06F1), RANKL and OPG (Abcam, Cat.  
423 ab269553 and ab203365) were measured by specific Elisa assays.

424

#### 425 **ACKNOWLEDGEMENTS**

426 This work was supported by grants from NIH grant (RF1, AG051538) to K. Y. The authors  
427 are thankful for Dr. Arthur W. English at Cell Biology Department at Emory University for  
428 critical proofreading the manuscript.

429

#### 430 **AUTHOR CONTRIBUTIONS**

431 K.Y. conceived the project, designed the experiments, analyzed the data and wrote the  
432 manuscript. X.J. designed and performed most of the experiments. X.L. prepared the animal  
433 breeding. J.A. performed the in vitro bone CT analysis. Z.Z. and R.P. contributed to write the  
434 manuscript.

435

#### 436 **COMPETING FINANCIAL INTERESTS**

437 The authors declare no competing financial interests.

439 **References:**

- 440 1 Huang, E. J. & Reichardt, L. F. Neurotrophins: roles in neuronal development and function. *Annu*  
 441 *Rev Neurosci* **24**, 677-736, doi:10.1146/annurev.neuro.24.1.677 (2001).
- 442 2 Kaplan, D. R. & Miller, F. D. Neurotrophin signal transduction in the nervous system. *Curr Opin*  
 443 *Neurobiol* **10**, 381-391, doi:10.1016/s0959-4388(00)00092-1 (2000).
- 444 3 Cartwright, M., Mikheev, A. M. & Heinrich, G. Expression of neurotrophin genes in human  
 445 fibroblasts: differential regulation of the brain-derived neurotrophic factor gene. *Int J Dev*  
 446 *Neurosci* **12**, 685-693, doi:10.1016/0736-5748(94)90048-5 (1994).
- 447 4 Labouyrie, E. *et al.* Expression of neurotrophins and their receptors in human bone marrow. *Am J*  
 448 *Pathol* **154**, 405-415, doi:10.1016/S0002-9440(10)65287-X (1999).
- 449 5 Simao, A. P. *et al.* Involvement of BDNF in knee osteoarthritis: the relationship with inflammation  
 450 and clinical parameters. *Rheumatol Int* **34**, 1153-1157, doi:10.1007/s00296-013-2943-5 (2014).
- 451 6 Kajiya, M. *et al.* Brain-derived neurotrophic factor stimulates bone/cementum-related protein  
 452 gene expression in cementoblasts. *J Biol Chem* **283**, 16259-16267, doi:10.1074/jbc.M800668200  
 453 (2008).
- 454 7 Kilian, O. *et al.* BDNF and its TrkB receptor in human fracture healing. *Ann Anat* **196**, 286-295,  
 455 doi:10.1016/j.aanat.2014.06.001 (2014).
- 456 8 Ida-Yonemochi, H., Yamada, Y., Yoshikawa, H. & Seo, K. Locally Produced BDNF Promotes  
 457 Sclerotic Change in Alveolar Bone after Nerve Injury. *PLoS One* **12**, e0169201,  
 458 doi:10.1371/journal.pone.0169201 (2017).
- 459 9 Dall, E. & Brandstetter, H. Structure and function of legumain in health and disease. *Biochimie*  
 460 **122**, 126-150, doi:10.1016/j.biochi.2015.09.022 (2016).
- 461 10 Choi, S. J. *et al.* Identification of human asparaginyl endopeptidase (legumain) as an inhibitor of  
 462 osteoclast formation and bone resorption. *J Biol Chem* **274**, 27747-27753,  
 463 doi:10.1074/jbc.274.39.27747 (1999).
- 464 11 Choi, S. J., Kurihara, N., Oba, Y. & Roodman, G. D. Osteoclast inhibitory peptide 2 inhibits  
 465 osteoclast formation via its C-terminal fragment. *J Bone Miner Res* **16**, 1804-1811,  
 466 doi:10.1359/jbmr.2001.16.10.1804 (2001).
- 467 12 Jafari, A. *et al.* Legumain Regulates Differentiation Fate of Human Bone Marrow Stromal Cells  
 468 and Is Altered in Postmenopausal Osteoporosis. *Stem Cell Reports* **8**, 373-386,  
 469 doi:10.1016/j.stemcr.2017.01.003 (2017).
- 470 13 Abdallah, B. M. & Kassem, M. Human mesenchymal stem cells: from basic biology to clinical  
 471 applications. *Gene Ther* **15**, 109-116, doi:10.1038/sj.gt.3303067 (2008).
- 472 14 Jang, S. W. *et al.* N-acetylserotonin activates TrkB receptor in a circadian rhythm. *Proc Natl Acad*  
 473 *Sci U S A* **107**, 3876-3881, doi:10.1073/pnas.0912531107 (2010).
- 474 15 Liu, X. *et al.* A synthetic 7,8-dihydroxyflavone derivative promotes neurogenesis and exhibits  
 475 potent antidepressant effect. *J Med Chem* **53**, 8274-8286, doi:10.1021/jm101206p (2010).
- 476 16 Liu, C., Chan, C. B. & Ye, K. 7,8-dihydroxyflavone, a small molecular TrkB agonist, is useful for  
 477 treating various BDNF-implicated human disorders. *Transl Neurodegener* **5**, 2,  
 478 doi:10.1186/s40035-015-0048-7 (2016).
- 479 17 Zhang, Z. *et al.* 7,8-dihydroxyflavone prevents synaptic loss and memory deficits in a mouse

480 model of Alzheimer's disease. *Neuropsychopharmacology* **39**, 638-650,  
481 doi:10.1038/npp.2013.243 (2014).

482 18 Devi, L. & Ohno, M. 7,8-dihydroxyflavone, a small-molecule TrkB agonist, reverses memory  
483 deficits and BACE1 elevation in a mouse model of Alzheimer's disease.  
484 *Neuropsychopharmacology* **37**, 434-444, doi:10.1038/npp.2011.191 (2012).

485 19 Castello, N. A. *et al.* 7,8-Dihydroxyflavone, a small molecule TrkB agonist, improves spatial  
486 memory and increases thin spine density in a mouse model of Alzheimer disease-like neuronal  
487 loss. *PLoS One* **9**, e91453, doi:10.1371/journal.pone.0091453 (2014).

488 20 Cikla, U. *et al.* ERalpha Signaling Is Required for TrkB-Mediated Hippocampal Neuroprotection in  
489 Female Neonatal Mice after Hypoxic Ischemic Encephalopathy(1,2,3). *eNeuro* **3**,  
490 doi:10.1523/ENEURO.0025-15.2015 (2016).

491 21 Chen, C. *et al.* The prodrug of 7,8-dihydroxyflavone development and therapeutic efficacy for  
492 treating Alzheimer's disease. *Proc Natl Acad Sci U S A* **115**, 578-583,  
493 doi:10.1073/pnas.1718683115 (2018).

494 22 Chen, C. *et al.* Gut dysbiosis contributes to amyloid pathology, associated with C/EBPbeta/AEP  
495 signaling activation in Alzheimer's disease mouse model. *Sci Adv* **6**, eaba0466,  
496 doi:10.1126/sciadv.aba0466 (2020).

497 23 Ren, E. *et al.* Functional and Structural Impairments in the Perirhinal Cortex of a Mouse Model of  
498 CDKL5 Deficiency Disorder Are Rescued by a TrkB Agonist. *Front Cell Neurosci* **13**, 169,  
499 doi:10.3389/fncel.2019.00169 (2019).

500 24 Wang, Z. H. *et al.* BDNF inhibits neurodegenerative disease-associated asparaginyl  
501 endopeptidase activity via phosphorylation by AKT. *JCI Insight* **3**, doi:10.1172/jci.insight.99007  
502 (2018).

503 25 Wang, Z. H. *et al.* C/EBPbeta regulates delta-secretase expression and mediates pathogenesis in  
504 mouse models of Alzheimer's disease. *Nat Commun* **9**, 1784, doi:10.1038/s41467-018-04120-z  
505 (2018).

506 26 Wang, Z. H. *et al.* Deficiency in BDNF/TrkB Neurotrophic Activity Stimulates delta-Secretase by  
507 Upregulating C/EBPbeta in Alzheimer's Disease. *Cell Rep* **28**, 655-669 e655,  
508 doi:10.1016/j.celrep.2019.06.054 (2019).

509 27 Compston, J. E., McClung, M. R. & Leslie, W. D. Osteoporosis. *Lancet* **393**, 364-376,  
510 doi:10.1016/S0140-6736(18)32112-3 (2019).

511 28 Windisch, J. M., Marksteiner, R., Lang, M. E., Auer, B. & Schneider, R. Brain-derived neurotrophic  
512 factor, neurotrophin-3, and neurotrophin-4 bind to a single leucine-rich motif of TrkB.  
513 *Biochemistry* **34**, 11256-11263, doi:10.1021/bi00035a035 (1995).

514 29 Liu, X. *et al.* Biochemical and biophysical investigation of the brain-derived neurotrophic factor  
515 mimetic 7,8-dihydroxyflavone in the binding and activation of the TrkB receptor. *J Biol Chem*  
516 **289**, 27571-27584, doi:10.1074/jbc.M114.562561 (2014).

517 30 Chan, C. B. *et al.* Activation of muscular TrkB by its small molecular agonist 7,8-dihydroxyflavone  
518 sex-dependently regulates energy metabolism in diet-induced obese mice. *Chem Biol* **22**, 355-  
519 368, doi:10.1016/j.chembiol.2015.02.003 (2015).

520 31 Fu, Q., Jilka, R. L., Manolagas, S. C. & O'Brien, C. A. Parathyroid hormone stimulates receptor  
521 activator of NFkappa B ligand and inhibits osteoprotegerin expression via protein kinase A  
522 activation of cAMP-response element-binding protein. *J Biol Chem* **277**, 48868-48875,  
523 doi:10.1074/jbc.M208494200 (2002).

524 32 Kondo, T., Kitazawa, R., Yamaguchi, A. & Kitazawa, S. Dexamethasone promotes  
525 osteoclastogenesis by inhibiting osteoprotegerin through multiple levels. *J Cell Biochem* **103**,  
526 335-345, doi:10.1002/jcb.21414 (2008).

527 33 Song, C. *et al.* Evaluation of efficacy on RANKL induced osteoclast from RAW264.7 cells. *J Cell*  
528 *Physiol* **234**, 11969-11975, doi:10.1002/jcp.27852 (2019).

529 34 Camerino, C. *et al.* Central depletion of brain-derived neurotrophic factor in mice results in high  
530 bone mass and metabolic phenotype. *Endocrinology* **153**, 5394-5405, doi:10.1210/en.2012-  
531 1378 (2012).

532 35 Charatcharoenwitthaya, N., Khosla, S., Atkinson, E. J., McCready, L. K. & Riggs, B. L. Effect of  
533 blockade of TNF-alpha and interleukin-1 action on bone resorption in early postmenopausal  
534 women. *J Bone Miner Res* **22**, 724-729, doi:10.1359/jbmr.070207 (2007).

535 36 Poli, V. The role of C/EBP isoforms in the control of inflammatory and native immunity functions.  
536 *J Biol Chem* **273**, 29279-29282, doi:10.1074/jbc.273.45.29279 (1998).

537 37 Ahn, E. H. *et al.* BDNF and Netrin-1 repression by C/EBPbeta in the gut triggers Parkinson's  
538 disease pathologies, associated with constipation and motor dysfunctions. *Prog Neurobiol* **198**,  
539 101905, doi:10.1016/j.pneurobio.2020.101905 (2021).

540 38 Kang, S. S. *et al.* TrkB neurotrophic activities are blocked by alpha-synuclein, triggering  
541 dopaminergic cell death in Parkinson's disease. *Proc Natl Acad Sci U S A* **114**, 10773-10778,  
542 doi:10.1073/pnas.1713969114 (2017).

543 39 Xiang, J. *et al.* Delta-secretase-cleaved Tau antagonizes TrkB neurotrophic signalings, mediating  
544 Alzheimer's disease pathologies. *Proc Natl Acad Sci U S A* **116**, 9094-9102,  
545 doi:10.1073/pnas.1901348116 (2019).

546 40 Suda, T. *et al.* Regulatory roles of beta-catenin and AP-1 on osteoprotegerin production in  
547 interleukin-1alpha-stimulated periodontal ligament cells. *Oral Microbiol Immunol* **24**, 384-389,  
548 doi:10.1111/j.1399-302X.2009.00529.x (2009).

549 41 Zhao, Z. *et al.* Crosstalk between the muscular estrogen receptor alpha and BDNF/TrkB signaling  
550 alleviates metabolic syndrome via 7,8-dihydroxyflavone in female mice. *Mol Metab* **45**, 101149,  
551 doi:10.1016/j.molmet.2020.101149 (2021).

552 42 Sun, L. *et al.* FSH directly regulates bone mass. *Cell* **125**, 247-260, doi:10.1016/j.cell.2006.01.051  
553 (2006).

554 43 Zhu, L. L. *et al.* Blocking antibody to the beta-subunit of FSH prevents bone loss by inhibiting  
555 bone resorption and stimulating bone synthesis. *Proc Natl Acad Sci U S A* **109**, 14574-14579,  
556 doi:10.1073/pnas.1212806109 (2012).

557 44 Shirahama-Noda, K. *et al.* Biosynthetic processing of cathepsins and lysosomal degradation are  
558 abolished in asparaginyl endopeptidase-deficient mice. *J Biol Chem* **278**, 33194-33199,  
559 doi:10.1074/jbc.M302742200 (2003).

560 45 Li, J. Y. *et al.* Sex steroid deficiency-associated bone loss is microbiota dependent and prevented  
561 by probiotics. *J Clin Invest* **126**, 2049-2063, doi:10.1172/JCI86062 (2016).

562 46 Li, J. Y. *et al.* IL-17A Is Increased in Humans with Primary Hyperparathyroidism and Mediates  
563 PTH-Induced Bone Loss in Mice. *Cell metabolism* **22**, 799-810, doi:10.1016/j.cmet.2015.09.012  
564 (2015).

565 47 Dempster, D. W. *et al.* Standardized nomenclature, symbols, and units for bone  
566 histomorphometry: a 2012 update of the report of the ASBMR Histomorphometry Nomenclature  
567 Committee. *J Bone Miner Res* **28**, 2-17, doi:10.1002/jbmr.1805 (2013).



568

569 **Figure legend**

570 **Figure 1. AEP knockout improves trabecular bone density in ovariectomy female mice.**

571 Femoral bone structures were assessed by *in vitro*  $\mu$ CT in AEP wild-type, AEP Knockout  
572 (AEP KO) mice with or without ovariectomy for 8 weeks. (A) Images of the femoral indices  
573 of trabecular bone structure measured by *in vitro*  $\mu$ CT scan. (B)  $\mu$ CT scanning measurements  
574 of trabecular bone volume fraction (BV/TV), Conn.D., Structure model index (SMI),  
575 Trabecular number (Tb.N), Trabecular spacing (Tb.Sp), trabecular thickness (Tb.Th). (n = 5  
576 to 7 mice per group, mean  $\pm$  SEM, one-way ANOVA, \* $P$ <0.05, \*\*  $P$ <0.01). (C) OVX-induced  
577 RANKL/OPG ratio is reduced in AEP KO mice. Serum levels of osteocalcin (a marker of  
578 bone formation), CTX (a marker of bone resorption), RANK-L, OPG, RANK-L/OPG ratio  
579 and serum BDNF level. (n = 5 to 7 mice per group, mean  $\pm$  SEM, one-way ANOVA,  
580 \* $P$ <0.05, \*\*  $P$ <0.01)

581

582 **Figure 2. AEP knockout inhibits the bone turnover induced by ovariectomy in female**  
583 **mice.**

584 (A) Hematoxylin and eosin (H&E) staining of the distal femur bone in AEP WT sham, AEP  
585 KO sham, AEP WT OVX and AEP KO OVX group. (Scale bar, 500  $\mu$ m). (B) Tartrate  
586 resistant acid phosphatase-stained (TRAP-stained) sections of the distal femur bone in AEP  
587 WT sham, AEP KO sham, AEP WT OVX and AEP KO OVX group were shown at low  
588 magnification (upper panel) and higher magnification (lower panel). (Scale bar, 500  $\mu$ m  
589 (upper panel), 20  $\mu$ m (lower panel)). (C) Mice were injected subcutaneously with calcein at

590 day 10 and day 3 before sacrifice. Trabecular calcein double-fluorescence labeling images of  
591 the representative sections in AEP WT sham, AEP KO sham, AEP WT OVX and AEP KO  
592 OVX group (Original magnification  $\times 20$ ). (D) Histomorphometric indices of bone turnover  
593 in AEP WT and AEP Knockout mice with or without ovariectomy. MAR and BFR/BS are  
594 indices of bone formation, N.Oc/BS and Oc.S/BS are indices of bone resorption. N.Ob/BS,  
595 Ob.S/BS are indices of bone formation. MAR = mineral apposition rate; BFR/BS = Bone  
596 formation rate; Ob.s/BS = percentage of bone surface covered by osteoblasts; N.Ob/BS =  
597 number of osteoblasts per mm bone surface; Oc.S/BS = percentage of bone surface covered  
598 by osteoclasts; N.Oc/BS = number of osteoclasts per mm bone surface. (n = 6 mice per  
599 group, mean  $\pm$  SEM, one-way ANOVA, \* $P < 0.05$ , \*\*  $P < 0.01$ )

600

601 **Figure 3. R13 treatment increases serum OPG levels and blocks trabecular bone loss**  
602 **induced by ovariectomy in both WT and BDNF+/- female mice.**

603 Femoral bone structures were assessed by *in vitro*  $\mu$ CT in wild-type, TrkB+/- and BDNF+/-  
604 mice (12 weeks old) with or without ovariectomy, and some of which administrated by R13  
605 (21.8 mg/kg) treatment for 8 weeks (6 days per week) by oral gavage. (A) Images of the  
606 femoral indices of trabecular bone structure measured by *in vitro*  $\mu$ CT scan. (B)  $\mu$ CT  
607 scanning measurements of trabecular bone volume fraction (BV/TV), Conn.D., Structure  
608 model index (SMI), Trabecular number (Tb.N), Trabecular spacing (Tb.Sp), trabecular  
609 thickness (Tb.Th). (n = 8 to 9 mice per group, mean  $\pm$  SEM, one-way ANOVA, \* $P < 0.05$ , \*\*  
610  $P < 0.01$ ). (C) R13 decreases RANKL/OPG ratio induced by OVX. Serum levels of  
611 osteocalcin, CTX, RANK-L, OPG, RANK-L/OPG ratio and serum BDNF levels. (n = 5 to 7

612 mice per group, mean  $\pm$  SEM, one-way ANOVA, \* $P$ <0.05, \*\*  $P$ <0.01)

613

614 **Figure 4. R13 treatment blocks the changes in bone turnover induced by ovariectomy in**  
615 **female mice.**

616 (A) Hematoxylin and eosin (H&E) staining of the distal femur bone in WT sham, BDNF +/-  
617 sham, WT OVX, BDNF +/- OVX, and WT OVX + R13, BDNF +/- OVX + R13 group.

618 (Scale bar, 500  $\mu$ m). (B) Tartrate resistant acid phosphatase-stained (TRAP-stained) sections

619 of the distal femur bone in WT sham, BDNF +/- sham, WT OVX, BDNF +/- OVX, and WT

620 OVX + R13, BDNF +/- OVX + R13 group were shown at low magnification (upper panel)

621 and higher magnification (lower panel). (Scale bar, 500  $\mu$ m (upper two panels), 20  $\mu$ m (lower

622 two panels)). (C) Mice were injected subcutaneously with calcein at day 10 and day 3 before

623 sacrifice. Trabecular calcein double-fluorescence labeling images of the representative

624 sections in WT sham, BDNF +/- sham, WT OVX, BDNF +/- OVX, and WT OVX + R13,

625 BDNF +/- OVX + R13 group (Original magnification  $\times$  20). (D) Histomorphometric indices

626 of bone turnover in WT and BDNF +/- mice after OVX with or without R13 treatment.

627 N.Oc/BS and Oc.S/BS are indices of bone resorption. N.Ob/BS, Ob.S/BS, MAR and BFR/BS

628 are indices of bone formation. (n = 6 mice per group, mean  $\pm$  SEM, one-way ANOVA,

629 \* $P$ <0.05, \*\*  $P$ <0.01). (E) The schematic diagram of the effect of R13 on osteoporosis.

630

631 **Figure 5. 7,8-DHF promotes MC3T3-E4 cells differentiation, mineralization and OPG**  
632 **secretion.**

633 (A) ALP staining in MC3T3-E4 cells treated with BDNF or 7,8-DHF for 14 days. (B)

634 Alizarin Red S mediated calcium staining in MC3T3-E4 cells treated with BDNF or 7,8-DHF  
635 for 21 days showed that 7,8-DHF promoted MC3T3 cells mineralization. (C) MC3T3 cells  
636 were cultured in complete medium or osteogenic induction medium (OIM) with BDNF or 7,8  
637 DHF for 4 days. Western blotting results showed 7,8-DHF inhibited C/EBP $\beta$ /AEP pathway  
638 and increase OPG expression. (D) Relative protein level of C/EBP $\beta$ , p-C/EBP $\beta$ , AEP,  
639 RANKL and OPG in MC3T3 cells cultured in complete medium or OIM with BDNF or 7,8  
640 DHF for 4 days; (E) AEP enzymatic activity assay. BDNF and 7,8-DHF inhibited AEP  
641 activity. Data represent mean  $\pm$  SEM of 3 independent experiments (\* $P$ <0.05, \*\*  $P$ <0.01, one-  
642 way ANOVA). (F) qPCR results showed that OPG mRNA expression increased in MC3T3  
643 cells after 7,8-DHF treatment for 4 days. Data represent mean  $\pm$  SEM of 3 independent  
644 experiments (\* $P$ <0.05, \*\*  $P$ <0.01, one-way ANOVA). (G) 7,8-DHF increases OPG and  
645 decreases RANKL/OPG ratio. Levels of OPG and RANK-L protein secreted into the medium  
646 were measured by ELISA. Data represent mean  $\pm$  SEM of 3 independent experiments  
647 (\* $P$ <0.05, \*\*  $P$ <0.01, one-way ANOVA).

648

649 **Figure 6. 7,8-DHF positively regulates OPG expression via activating CREB.**

650 (A) MC3T3 cells cultured in OIM were treated with 7,8-DHF in different time points.  
651 Western blotting showed that 7,8-DHF inhibited C/EBP $\beta$ , increased AKT (S473), MAPK  
652 (p38), C-Jun, CREB phosphorylation. (B) Relative protein level of C/EBP $\beta$ , p- C/EBP $\beta$ ,  
653 AEP, phosphorylated C-Jun, CREB, AKT, MAPK and TrkB in MC3T3 cells treated with 7,8-  
654 DHF in different time points. Data represent mean  $\pm$  SEM of 3 independent experiments  
655 (\* $P$ <0.05, \*\*  $P$ <0.01, one-way ANOVA). (C) Western blotting showed that knockdown of

656 CREB blunted 7,8-DHF-induced OPG expression. (D) Relative protein level of RANKL,  
657 OPG and RANKL/OPG ratio. Data represent mean  $\pm$  SEM of 3 independent experiments  
658 (\* $P$ <0.05, \*\*  $P$ <0.01, one-way ANOVA). (E) qPCR results showed that knockdown of CREB  
659 inhibited OPG mRNA expression induced by 7,8-DHF. Data represent mean  $\pm$  SEM of 3  
660 independent experiments (\* $P$ <0.05, \*\*  $P$ <0.01, one-way ANOVA).

661

662

663 **Supplementary Figure 1. Ovariectomy induced uterus atrophy in wild type mice.**

664 (A) The uterus morphology of the wild-type mice with or without ovariectomy. (B) Uterus  
665 weight of the wild-type mice with or without ovariectomy.

666

667 **Supplementary Figure 2. R13 increases trabecular bone density in wild-type mice.**

668 WT mice were treated with or without R13 (21.8 mg/kg) for 8 weeks (6 days per week) by  
669 oral gavage at 3 months old. Femoral bone structures were assessed by *in vitro*  $\mu$ CT. (A)  
670 Images of the femoral indices of trabecular bone structure measured by *in vitro*  $\mu$ CT scan. (B)  
671 R13 increases bone volume fraction in WT mice.  $\mu$ CT scanning measurements of trabecular  
672 bone volume fraction (BV/TV), Conn.D., Structure model index (SMI), Trabecular number  
673 (Tb.N), Trabecular spacing (Tb.Sp), trabecular thickness (Tb.Th). (n = 8 mice per group,  
674 mean  $\pm$  SEM, one-way ANOVA, \* $P$ <0.05, \*\*  $P$ <0.01). (C) R13 elevates OPG levels in WT  
675 mice. Serum levels of Osteocalcin, CTX, RANK-L, OPG, RANK-L/OPG ratio and serum  
676 BDNF levels. (n = 5 to 7 mice per group, mean  $\pm$  SEM, one-way ANOVA, \* $P$ <0.05, \*\*  
677  $P$ <0.01).

678

679 **Supplementary figure 3. Blocking AEP activity promotes MC3T3-E4 cell differentiation**  
680 **and mineralization.**

681 MC3T3 cells were cultured in OIM and transfected with or without AEP<sup>C189S</sup> plasmid. (A)  
682 Western blot showed that AEP<sup>C189S</sup> transfection increased fibronectin, osterix, RUNX2 and  
683 phosphorylated-CREB expression. (B) AEP<sup>C189S</sup> transfection increased ALP staining positive  
684 cells in MC3T3 cells cultured in OIM for 14 days. (C) Alizarin Red S mediated calcium  
685 staining in MC3T3-E4 cells treated with or without AEP<sup>C189S</sup> transfection for 21 days. (D)  
686 Relative protein level of AEP, fibronectin, osterix, runx2 and p-CREB/CREB. Data represent  
687 mean ± SEM of 3 independent experiments (\**P*<0.05, \*\**P*<0.01, one-way ANOVA). (E)  
688 AEP<sup>C189S</sup> transfection inhibited AEP activity in MC3T3-E4 cells cultured in OIM.

689

690 **Supplementary Figure 4. 7,8-DHF inhibits RANK-L-induced RAW264.7**  
691 **osteoclastogenesis.**

692 (A) TRAP staining of RAW 264.7 cells induced by RANKL with or without BDNF or 7,8-  
693 DHF for 4 days. (B& C) Western blotting showed that BDNF and 7,8-DHF inhibited  
694 C/EBPβ/AEP pathway, and activated p-TrkB and p-MAPK and p-AKT signaling.

695

696

697

# Figures

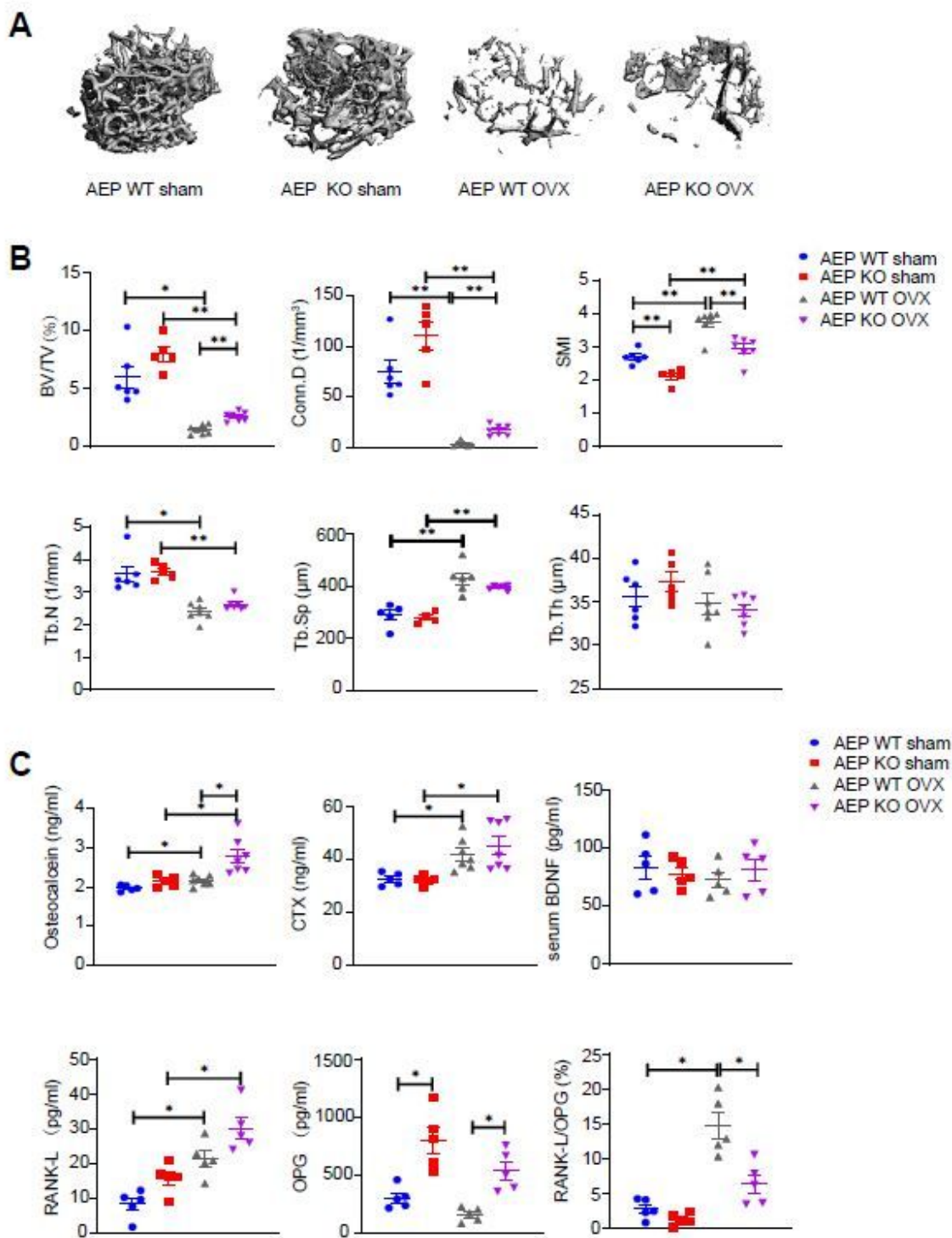


**Figure 1**

AEP knockout improves trabecular bone density in ovariectomy female mice. Femoral bone structures were assessed by in vitro  $\mu$ CT in AEP wild-type, AEP Knockout (AEP KO) mice with or without ovariectomy for 8 weeks. (A) Images of the femoral indices of trabecular bone structure measured by in vitro  $\mu$ CT

scan. (B)  $\mu$ CT scanning measurements of trabecular bone volume fraction (BV/TV), Conn.D., Structure model index (SMI), Trabecular number (Tb.N), Trabecular spacing (Tb.Sp), trabecular thickness (Tb.Th). (n = 5 to 7 mice per group, mean  $\pm$  SEM, one-way ANOVA, \*P<0.05, \*\* P<0.01). (C) OVX-induced RANKL/OPG ratio is reduced in AEP KO mice. Serum levels of osteocalcin (a marker of bone formation), CTX (a marker of bone resorption), RANK-L, OPG, RANK-L/OPG ratio and serum BDNF level. (n = 5 to 7 mice per group, mean  $\pm$  SEM, one-way ANOVA, \*P<0.05, \*\* P<0.01)

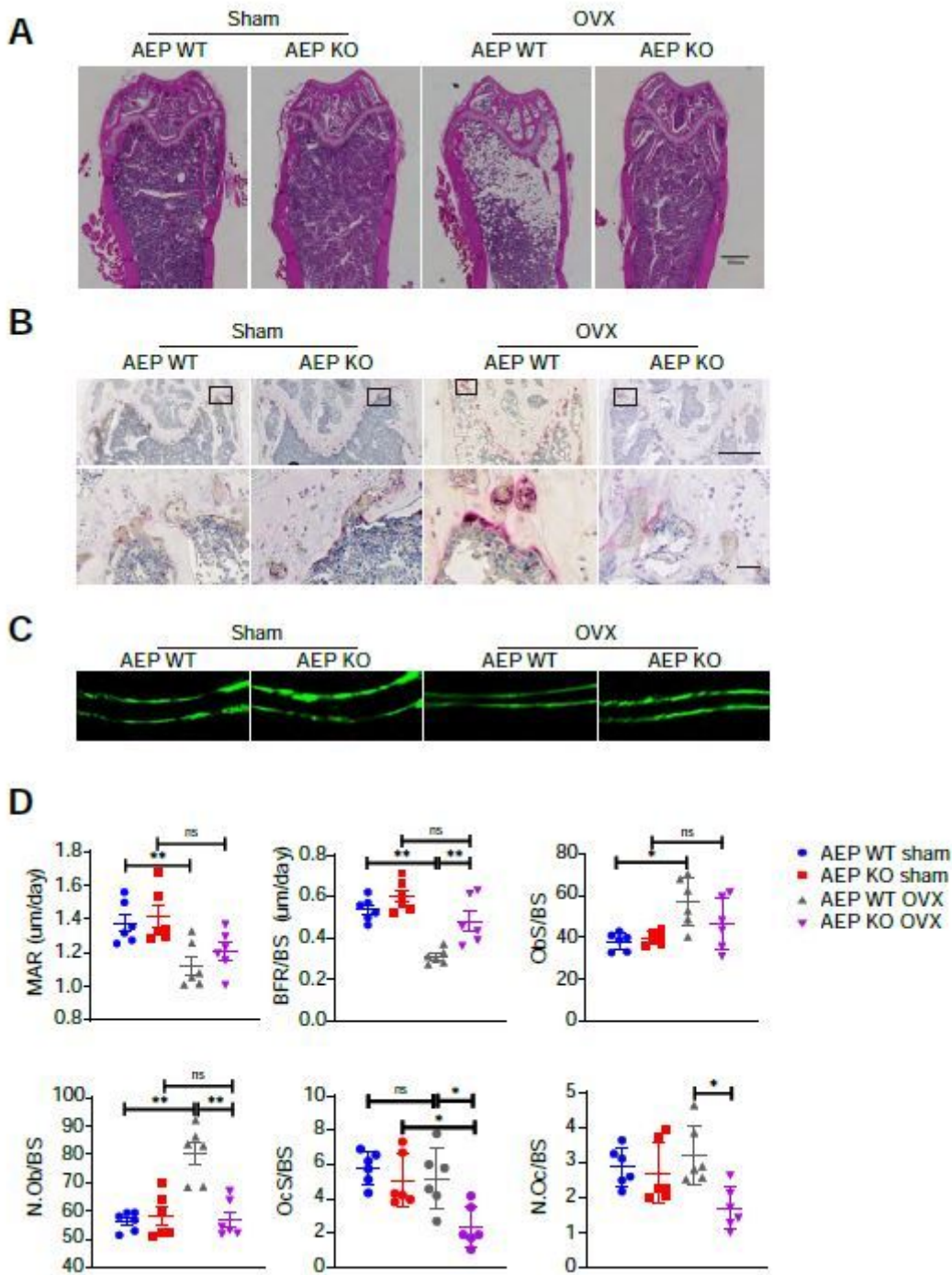
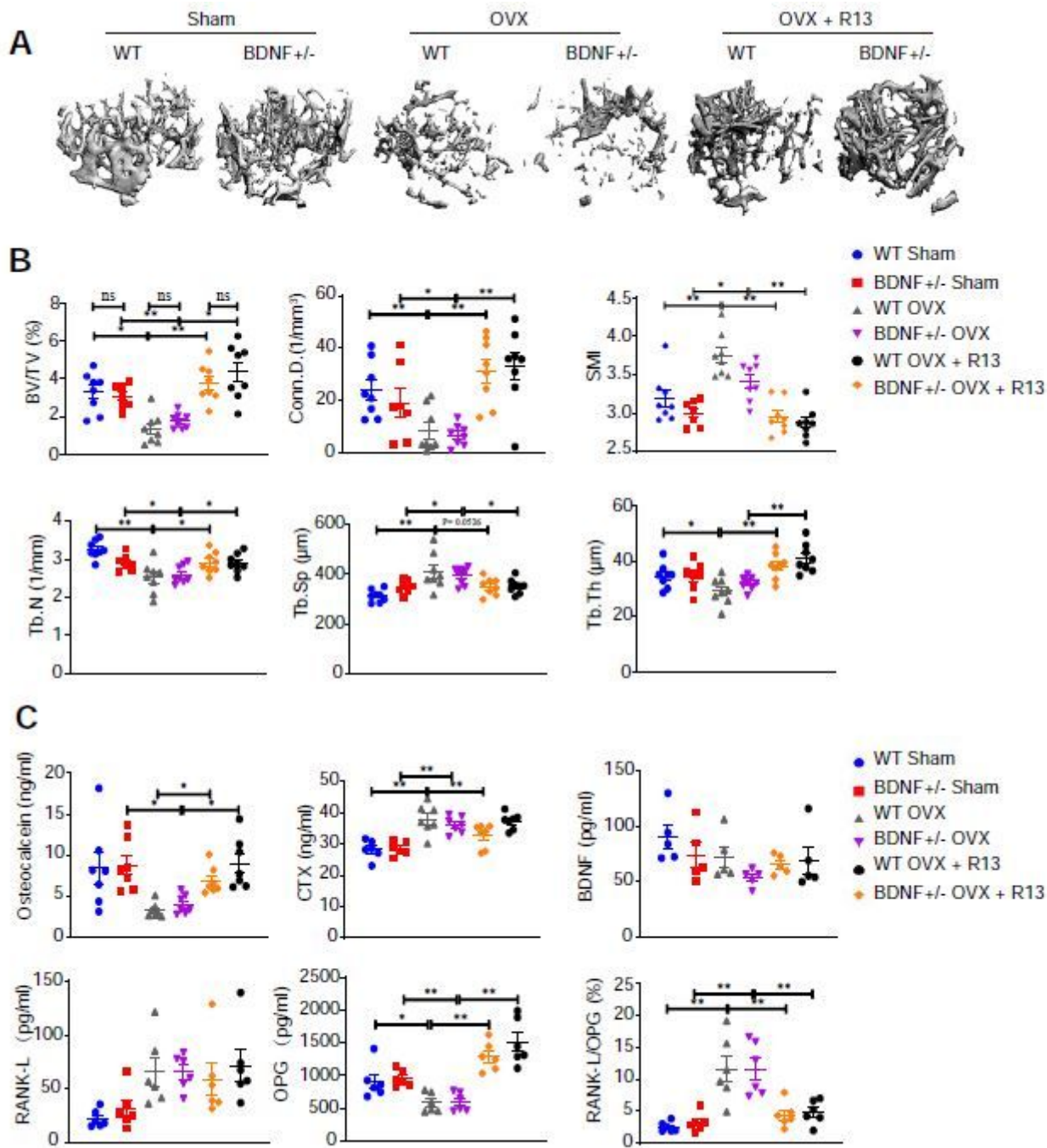


Figure 2



AEP knockout inhibits the bone turnover induced by ovariectomy in female 582 mice. (A) Hematoxylin and eosin (H&E) staining of the distal femur bone in AEP WT sham, AEP KO sham, AEP WT OVX and AEP KO OVX group. (Scale bar, 500  $\mu\text{m}$ ). (B) Tartrate resistant acid phosphatase-stained (TRAP-stained) sections of the distal femur bone in AEP WT sham, AEP KO sham, AEP WT OVX and AEP KO OVX group were shown at low magnification (upper panel) and higher magnification (lower panel). (Scale bar, 500  $\mu\text{m}$  (upper panel), 20  $\mu\text{m}$  (lower panel)). (C) Mice were injected subcutaneously with calcein at 25 day 10 and day 3 before sacrifice. Trabecular calcein double-fluorescence labeling images of the representative sections in AEP WT sham, AEP KO sham, AEP WT OVX and AEP KO OVX group (Original magnification  $\times 20$ ). (D) Histomorphometric indices of bone turnover in AEP WT and AEP Knockout mice with or without ovariectomy. MAR and BFR/BS are indices of bone formation, N.Oc/BS and Oc.S/BS are indices of bone resorption. N.Ob/BS, Ob.S/BS are indices of bone formation. MAR = mineral apposition rate; BFR/BS = Bone formation rate; Ob.s/BS = percentage of bone surface covered by osteoblasts; N.Ob/BS = 596 number of osteoblasts per mm bone surface; Oc.S/BS = percentage of bone surface covered by osteoclasts; N.Oc/BS = number of osteoclasts per mm bone surface. (n = 6 mice per group, mean  $\pm$  SEM, one-way ANOVA, \*P<0.05, \*\* P<0.01)



**Figure 3**

R13 treatment increases serum OPG levels and blocks trabecular bone loss induced by ovariectomy in both WT and BDNF<sup>+/-</sup> female mice. Femoral bone structures were assessed by in vitro  $\mu$ CT in wild-type, TrkB<sup>+/-</sup> and BDNF<sup>+/-</sup> mice (12 weeks old) with or without ovariectomy, and some of which administrated by R13 (21.8 mg/kg) treatment for 8 weeks (6 days per week) by oral gavage. (A) Images of the femoral indices of trabecular bone structure measured by in vitro  $\mu$ CT scan. (B)  $\mu$ CT scanning measurements of trabecular bone volume fraction (BV/TV), Conn.D., Structure model index (SMI), Trabecular number (Tb.N), Trabecular spacing (Tb.Sp), trabecular thickness (Tb.Th). (n = 8 to 9 mice per group, mean  $\pm$  SEM,

one-way ANOVA, \* $P < 0.05$ , \*\*  $P < 0.01$ ). (C) R13 decreases RANKL/OPG ratio induced by OVX. Serum levels of osteocalcin, CTX, RANK-L, OPG, RANK-L/OPG ratio and serum BDNF levels. (n = 5 to 7 26 mice per group, mean  $\pm$  SEM, one-way ANOVA, \* $P < 0.05$ , \*\*  $P < 0.01$ )

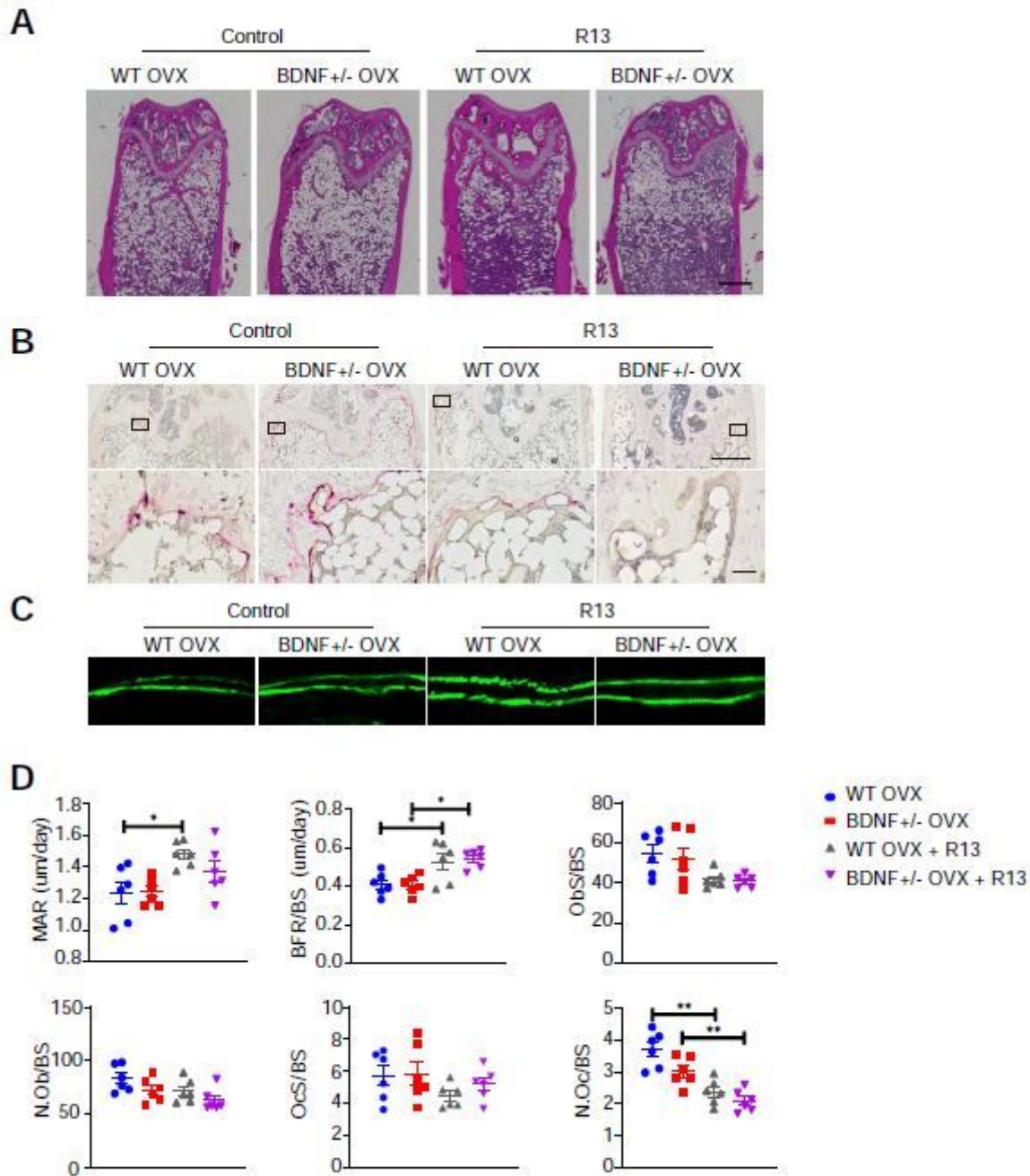


**Figure 4**

R13 treatment blocks the changes in bone turnover induced by ovariectomy in female mice. (A) Hematoxylin and eosin (H&E) staining of the distal femur bone in WT sham, BDNF +/- sham, WT OVX, BDNF +/- OVX, and WT OVX + R13, BDNF +/- OVX + R13 group. (Scale bar, 500  $\mu$ m). (B) Tartrate resistant acid phosphatase-stained (TRAP-stained) sections of the distal femur bone in WT sham, BDNF +/- sham,

WT OVX, BDNF +/- OVX, and WT OVX + R13, BDNF +/- OVX + R13 group were shown at low magnification (upper panel) and higher magnification (lower panel). (Scale bar, 500  $\mu\text{m}$  (upper two panels), 20  $\mu\text{m}$  (lower two panels)). (C) Mice were injected subcutaneously with calcein at day 10 and day 3 before sacrifice. Trabecular calcein double-fluorescence labeling images of the representative sections in WT sham, BDNF +/- sham, WT OVX, BDNF +/- OVX, and WT OVX + R13, BDNF +/- OVX + R13 group (Original magnification  $\times 20$ ). (D) Histomorphometric indices of bone turnover in WT and BDNF +/- mice after OVX with or without R13 treatment. N.Oc/BS and Oc.S/BS are indices of bone resorption. N.Ob/BS, Ob.S/BS, MAR and BFR/BS are indices of bone formation. (n = 6 mice per group, mean  $\pm$  SEM, one-way ANOVA, \*P<0.05, \*\* P<0.01). (E) The schematic diagram of the effect of R13 on osteoporosis.

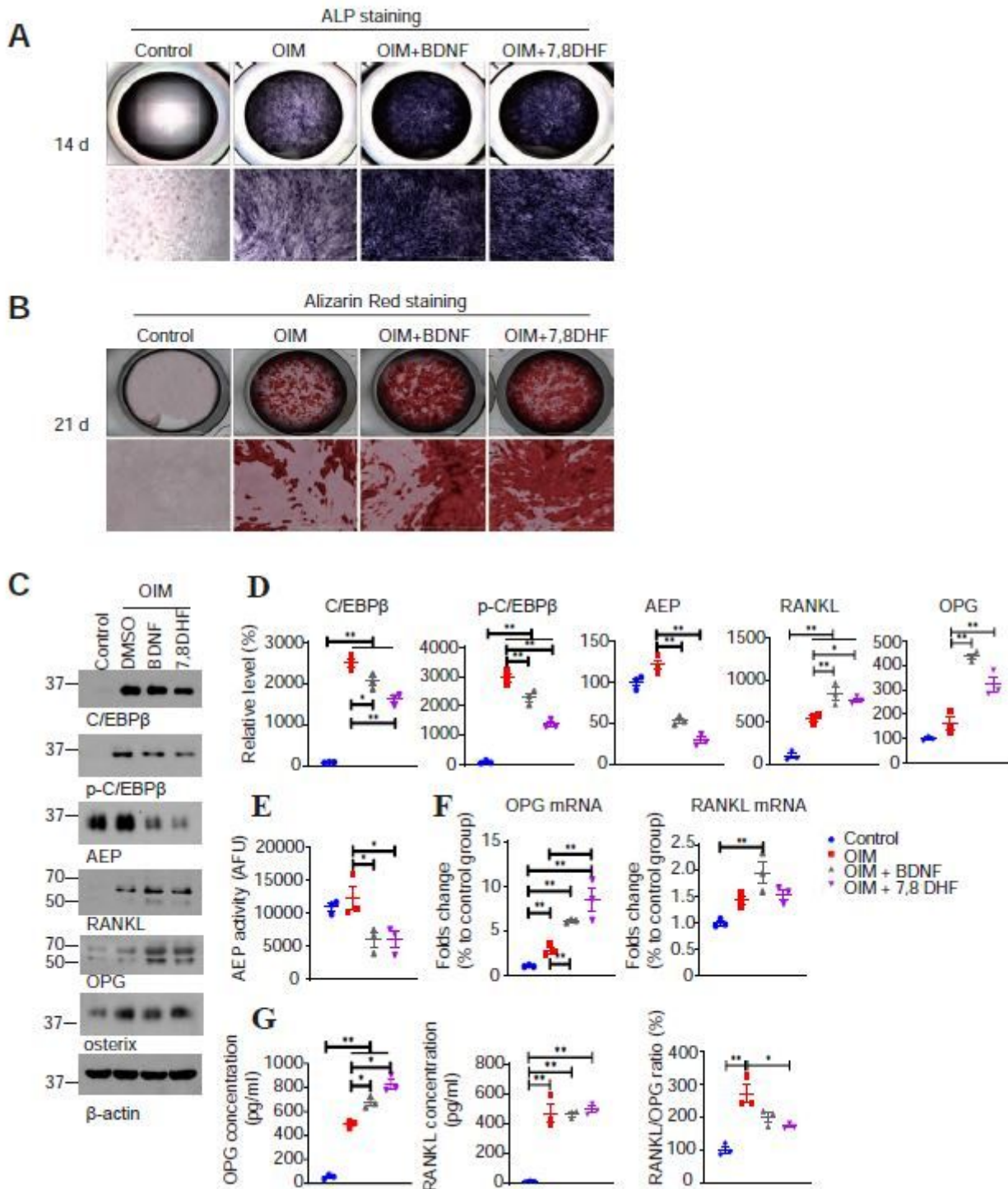


**Figure 5**

7,8-DHF promotes MC3T3-E4 cells differentiation, mineralization and OPG secretion. (A) ALP staining in MC3T3-E4 cells treated with BDNF or 7,8-DHF for 14 days. (B) 27 Alizarin Red S mediated calcium staining in MC3T3-E4 cells treated with BDNF or 7,8-DHF for 21 days showed that 7,8-DHF promoted MC3T3 cells mineralization. (C) MC3T3 cells were cultured in complete medium or osteogenic induction medium (OIM) with BDNF or 7,8 DHF for 4 days. Western blotting results showed 7,8-DHF inhibited

C/EBP $\beta$ /AEP pathway and increase OPG expression. (D) Relative protein level of C/EBP $\beta$ , p-C/EBP $\beta$ , AEP, RANKL and OPG in MC3T3 cells cultured in complete medium or OIM with BDNF or 7,8 DHF for 4 days; (E) AEP enzymatic activity assay. BDNF and 7,8-DHF inhibited AEP activity. Data represent mean  $\pm$  SEM of 3 independent experiments (\*P<0.05, \*\* P<0.01, one-way ANOVA). (F) qPCR results showed that OPG mRNA expression increased in MC3T3 cells after 7,8-DHF treatment for 4 days. Data represent mean  $\pm$  SEM of 3 independent experiments (\*P<0.05, \*\* P<0.01, one-way ANOVA). (G) 7,8-DHF increases OPG and decreases RANKL/OPG ratio. Levels of OPG and RANK-L protein secreted into the medium 645 were measured by ELISA. Data represent mean  $\pm$  SEM of 3 independent experiments (\*P<0.05, \*\* P<0.01, one-way ANOVA).

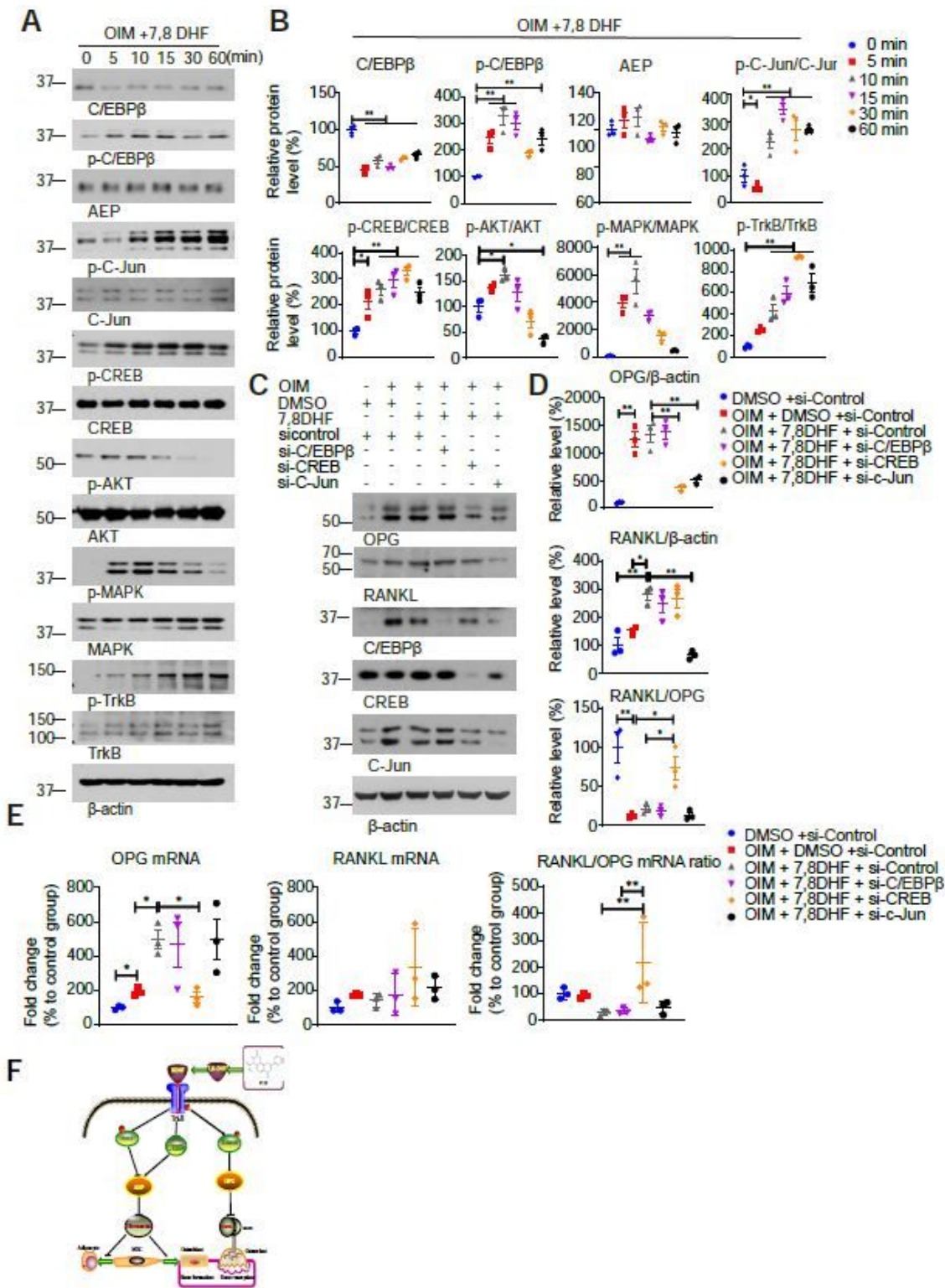


**Figure 6**

7,8-DHF positively regulates OPG expression via activating CREB. (A) MC3T3 cells cultured in OIM were treated with 7,8-DHF in different time points. Western blotting showed that 7,8-DHF inhibited C/EBPβ, increased AKT (S473), MAPK (p38), C-Jun, CREB phosphorylation. (B) Relative protein level of C/EBPβ, p-C/EBPβ, AEP, phosphorylated C-Jun, CREB, AKT, MAPK and TrkB in MC3T3 cells treated with 7,8-DHF in different time points. Data represent mean  $\pm$  SEM of 3 independent experiments (\* $P < 0.05$ , \*\*  $P < 0.01$ , one-

way ANOVA). (C) Western blotting showed that knockdown of CREB blunted 7,8-DHF-induced OPG expression. (D) Relative protein level of RANKL, OPG and RANKL/OPG ratio. Data represent mean  $\pm$  SEM of 3 independent experiments (\*P<0.05, \*\* P<0.01, one-way ANOVA). (E) qPCR results showed that knockdown of CREB inhibited OPG mRNA expression induced by 7,8-DHF. Data represent mean  $\pm$  SEM of 3 independent experiments (\*P<0.05, \*\* P<0.01, one-way ANOVA).